Luminescent Properties of Long-Lasting $BaAl_xO_y:Eu^{2+},Dy^{3+}$ Nanocomposites

Daniel B. Bem,[1,2] Hendrick C. Swart,[3] Adriaan S. Luyt,[4] Francis B. Dejene[1]

[1]*Department of Physics, University of the Free State (Qwaqwa Campus), Phuthaditjhaba, ZA9866, South Africa*
[2]*Department of Physics, Kenyatta University, P.O. Box 43844, 00100 GPO, Nairobi, Kenya*
[3]*Department of Physics, University of the Free State, P.O. Box 339, Bloemfontein, ZA9300, South Africa*
[4]*Department of Chemistry, University of the Free State (Qwaqwa Campus), Phuthaditjhaba, ZA9866, South Africa*

Received 3 October 2010; accepted 5 October 2010
DOI 10.1002/app.33553
Published online 17 February 2011 in Wiley Online Library (wileyonlinelibrary.com).

ABSTRACT: $BaAl_xO_y:Eu^{2+},Dy^{3+}$ blue-green phosphor samples were synthesized by a combustion method at the low temperature of 500°C. Phosphor nanocrystallites with high brightness were obtained without significantly changing the crystalline structure of the host. The crystallite sizes determined from the Scherrer equation ranged between 34 and 41 nm. Different volume fractions of the $BaAl_xO_y:Eu^{2+},Dy^{3+}$ powder were then introduced in LDPE polymer. The resulting composites were similarly analyzed and also thermally characterized by means of differential scanning calorimetry (DSC) and thermogravimetric analysis (TGA). PL results indicate that the LDPE-phosphor interface, which is considered to have an influence on the composite behavior, did not significantly change the spectral positions of the phosphor materials, whose major emission peaks occurred at about 505 nm. The improved afterglow results for the composites may have been caused by morphological changes due to increased surface area and defects. Thermal results indicate that the $BaAl_xO_y:Eu^{2+},Dy^{3+}$ particles acted as nucleating centers and enhanced the overall crystallinity in the LDPE nanocomposite while preventing lamellar growth, hence reducing the crystallite sizes in LDPE. © 2011 Wiley Periodicals, Inc. J Appl Polym Sci 121: 243–252, 2011

Key words: $BaAl_xO_y:Eu^{2+},Dy^{3+}$; long afterglow; nanocomposites

INTRODUCTION

Luminescent materials have attracted extensive attention due to the potential for application in various devices. They have been put to use as display materials and are currently in widespread use in applications of high definition television (HDTV), plasma display panels (PDP), cathode ray tubes (CRT), and field emission displays (FED).[1,2] Among these luminescent materials, rare earth doped phosphors are of technological importance and are widely used in color displays and fluorescent lamps.[3]

Extensive research on aluminate phosphors has been undertaken following the outstanding work by Matsuzawa et al.[4] who in 1996 reported for the first time the green and blue emitting long-lasting phosphorescent phenomenon from Eu^{2+}-doped and rare earth (R^{3+}) codoped alkaline earth aluminates ($MAl_2O_4:Eu^{2+},R^{3+}$; M: Ca and Sr).[4]

However, the Eu^{2+},R^{3+} codoped barium aluminates such as $BaAl_xO_y:Eu^{2+},Dy^{3+}$[5,6] have been studied only infrequently, even though they have potential for persistent luminescence. The reasons may be attributed to the rather complicated structural chemistry of the MAl_2O_4 host as well as the considerable size mismatch between the host (Ba^{2+}) and the main dopant (Eu^{2+}) cations.[7] On the other hand, the crystal structures of the compounds studied in this work are all derivatives of the stuffed tridymite structure. In this type of structure there are large open channels in the framework, which provide suitable sites for large cations. These channels are capable of weakening the phosphor structure, ultimately degrading it. Another inspiration to study these materials is the possibility to produce composites on the nano- or microscale with improved physical and chemical properties, which commonly differ from those of bulky materials.[8]

The optimization of properties for new and potentially useful materials becomes a continuous and

Correspondence to: H. C. Swart (dejenebf@qwa.ufs.ac.za or swarthc@ufs.ac.za).

Contract grant sponsors: University of the Free State in South Africa, The National Research Foundation.

sometimes a lifelong process if future applications are anticipated. In this study, $BaAl_2O_4:Eu^{2+},Dy^{3+}$ phosphor materials were prepared at different Eu^{2+} and Dy^{3+} concentrations by means of the combustion method.[9] A $BaAl_xO_y:Eu^{2+},Dy^{3+}$ phosphor with high brightness was successfully prepared. The effects of the Eu^{2+}:Dy^{3+} molar ratio on the structure, homogeneity, persistent luminescence as well as stability are presented and discussed based on the analyses of the x-ray powder diffraction, SEM imaging and luminescence spectroscopic studies. In addition to the synthesized $BaAl_xO_y:Eu^{2+},Dy^{3+}$ powder, polymer-phosphor composites of well-defined compositions were also prepared and studied. The motivation in the present work was twofold: (i) polymer-inorganic nanocrystal composites offer an attractive means to combine the merits of organic and inorganic materials into systems with novel properties. Hence, the emergence of polymer-nanoparticle composites as a class of materials for optoelectronic devices such as luminescent devices,[10] thin film transistors,[11] photovoltaic devices,[12] and optical waveguides[13]; and (ii) though work on polymer-phosphor nanocomposites is quite nascent, previous results so far obtained by this group[14] are quite promising. The results of the polymer-phosphor nanocomposites from the current work are also quite encouraging for practical applications.

EXPERIMENTAL

Experimental section

Synthesis of the $BaAl_xO_y:Eu^{2+},Dy^{3+}$phosphor samples

Barium aluminate samples were prepared by a combustion synthesis method. Powders of $Ba(NO_3)_2$ (A.R.), $Al(NO_3)_3{\cdot}9H_2O$ (A.R.), Eu_2 $(NO_3)_3$ (4*N*), CH_4N_2O (A.R. added as fuel) were used as starting materials. Eu^{3+} was introduced in the form of $Eu(NO_3)_3.5H_2O$. A homogeneous, thick white solution was obtained after thoroughly milling the precursor mixture in a mortar using a pestle. Formation of the solution was facilitated by the water of crystallization present on the metal nitrates. The solution was then introduced into a muffle furnace maintained at 500°C. Initially, the paste boiled and underwent dehydration, followed by decomposition with large amounts of gases escaping. Spontaneous ignition then occurred and the material underwent smouldering combustion with enormous swelling. The whole process was over in about 5 min. The voluminous and foamy combustion ash was easily milled to obtain the final $BaAl_xO_y:Eu^{2+},Dy^{3+}$ phosphor powder.

Preparation of $BaAl_xO_y:Eu^{2+},Dy^{3+}$-LDPE nanocomposites

Linear low-density polyethylene (LDPE) was supplied by Sasol Polymers, South Africa. It has a melt flow index (MFI) of 2.0 g/10 min, which was determined by preheating a sample of the polymer at 190°C for 5 min followed by a shear analysis on a 2.16 kg mass. It has a melting point of about 110°C, and a density of 0.922 g cm^{-3}. The polymer/phosphor composites were produced by melt-mixing the synthesized barium aluminate phosphor powder into LDPE at volume ratios ranging from 0.4 to 10%. Samples were weighed according to the required ratios and mixed using a volume of 50 cm^3 in a Brabender Plastograph mixing chamber at a speed of 30 rpm for 15 min. The mixing was carried out at 160°C. The samples were hot melt-pressed into slabs of average thickness 0.98 ± 0.05 mm, at 160°C.

Sample characterization

Morphology and structural analysis. Microstructural and elemental composition characterization of the $BaAl_xO_y:Eu^{2+},Dy^{3+}$particles were performed on a Shimadzu model ZU SSX-550 Superscan scanning electron microscope (SEM), coupled with an energy dispersive X-ray spectrometer (EDS). For SEM measurements, the probe size was 115 nm, the probe current 0.02 nA, and the accelerating voltage 5.0 keV. The probe size for EDS analysis was 4 nm, specimen current 1.00 nA, and accelerating voltage 15.0 keV.

Crystalline phases were characterized by an X-ray diffractometer (Bruker D8 diffractometer, Bruker Corp. of Germany, operating at 40 kV and 40 mA, and using Cu-K_α = 1.5406 Å) with a scan step of 0.02° in 2θ and a scan speed of 4°/min. The divergence slit (DS), scatter slit (SS), and receiving slit (RS) are 1°, 1°, and 0.15 mm, respectively. The average crystallite size of the materials was calculated from the diffraction data by using the Scherrer equation [eq. (1)],[15]

$$D = \frac{0.9\lambda}{\beta \cos\theta} \quad (1)$$

where D is the average crystallite size in meters, λ the X-ray wavelength in meters, β the full width at half maximum (FWHM) of the selected reflection in radians, and θ (in degrees) is half of the Bragg angle (2θ). The calculation is based on the measurement of full-width at half-maximum (FWHM) values in the corresponding XRD pattern. The broadening of the peaks due to the instrumental effect was also taken into account.

Photoluminescence (PL) measurements. The excitation, emission, and decay spectra were measured at room

temperature on a Cary Eclipse fluorescence spectrophotometer (Model: LS 55) with a built-in 150 W xenon lamp as the excitation source and a grating to select a suitable wavelength for excitation. Each sample was loaded into a circular holder and excited with 340 nm radiation.

Thermal analysis. Differential scanning calorimetric (DSC) analyses were performed on a Perkin–Elmer DSC7 thermal analyzer, under flowing nitrogen (20 mL min^{-1}). The system is interfaced to a computer, which was used for calculations by means of Pyris software. Samples averaging 7 mg were sealed in aluminum pans and heated from 25 to 160°C at a heating rate of 10°C min^{-1}, and immediately cooled at the same rate to 25°C. For the second scan, the samples were heated and cooled under the same conditions. Peak temperatures of melting and crystallization, as well as melting and crystallization enthalpies, were determined from the second scan, to eliminate the effect of history. Thermogravimetric analyses (TGA) were performed in a Perkin–Elmer TGA7 thermogravimetric analyzer in a flowing nitrogen atmosphere (20 mL min^{-1}). The samples (approximately 7 mg each) were heated from 25 to 600°C at a rate of 10°C min^{-1}. For both DSC and TGA analyses three measurements were performed on each sample composition, from which average temperature and enthalpy values were determined.

RESULTS AND DISCUSSION

SEM micrographs and EDS spectra

The microstructures of $BaAl_xO_y:Eu^{2+},Dy^{3+}$ powders are shown in the SEM micrographs in Figure 1. Figure 1(a,b) depict the SEM images of the as-synthesized phosphor powders for low (a) and high (b) Dy^{3+} concentrations, respectively. The magnification is 10,000× in both images. An inspection of the morphology of the as-synthesized powder samples reveal that the phosphor powders are characterized by flakes up to 10 μm diameter. The surface of the powder samples shows voids and pores formed by the escaping gases during the combustion process. When a gas is escaping under high pressure, pores are formed with the formation of small particles near the pores. The formed gas transports heat away from the forming product, thus limiting the particle growth. The wide particle-size distribution as well as irregular shapes of the particles is probably due to the nonuniform distribution of temperature and mass flow in the combustion wave.

Energy dispersive spectroscopy (EDS) is a standard procedure for identifying and quantifying elemental composition of sample areas as small as a few micrometres.[16] Figure 2 shows the EDS spectra of the sample with 10 : 1, Eu^{2+}:Dy^{3+} molar ratio. The existence of Eu in the samples is clear in their corresponding EDS spectra. There appeared no other emissions apart from Ba, Eu, O, Dy, Al, and C in the EDS spectra of the samples. The elements appear in ratios concomitant with the proportions mixed in the starting materials, which shows the advantage of the combustion method in controlling chemical components.

X-ray diffraction (XRD)

Generally, it is well known that the luminescence properties of phosphor particles are strongly dependent upon the characteristics of the prepared phosphors such as particle size,[17] surface morphology,[18] concentration quenching,[19] and crystallinity.[20] Crystallinity is one of the most important parameters to obtain the phosphor particles with high luminescence efficiency.

The X-ray powder diffraction (XRPD) technique is an effective tool for determining the phase, crystallinity, and purity of samples prepared under various conditions. Figure 3(a,b) is a display of the XRD results for the $BaAl_xO_y:Eu^{2+},Dy^{3+}$phosphors and $BaAl_xO_y:Eu^{2+},Dy^{3+}$/LDPE nanocomposite. The broad peaks clearly indicate that nanoparticles were obtained. The phosphor flakes therefore consist of agglomerated nanoparticles. The spectrum clearly shows the expected hexagonal crystalline phase for the nanopowders. The main diffraction peaks index well with the card file (JCPDS:17-0306) in agreement with other reports.[21,22] Crystallite size estimation based on the Scherrer analysis yielded average values ranging between 34 and 41 nm.

Photoluminescence spectra

PL measurements were carried out to determine the luminescent properties of the as-prepared aluminate phosphor samples as well as those of the LDPE/$BaAl_xO_y:Eu^{2+},Dy^{3+}$ nanocomposites. Figures 4 and 5 display the excitation and emission spectra for the phosphors and nanocomposites, respectively. The photoluminescence spectra exhibit different shapes and broadband peaks. The wavelength bands in the excitation are broad with wavelengths ranging from 275 to 445 nm while the corresponding blue-green emissions consist mainly of symmetrical bands with major peaks having maxima at 505 nm that originate from the energy transitions between the ground state ($4f^7$) and the excited state ($4f^65d^1$) of the Eu^{2+} ions.[23] The minor peaks at 615 and 685 nm arise from the f-f transitions of the remnant unreduced Eu^{3+} ions.

The photoluminescence in rare earth-doped alkaline earth aluminates originates in the electronic transitions in the rare earth ions. The luminescence may be attributed to one of three possible processes

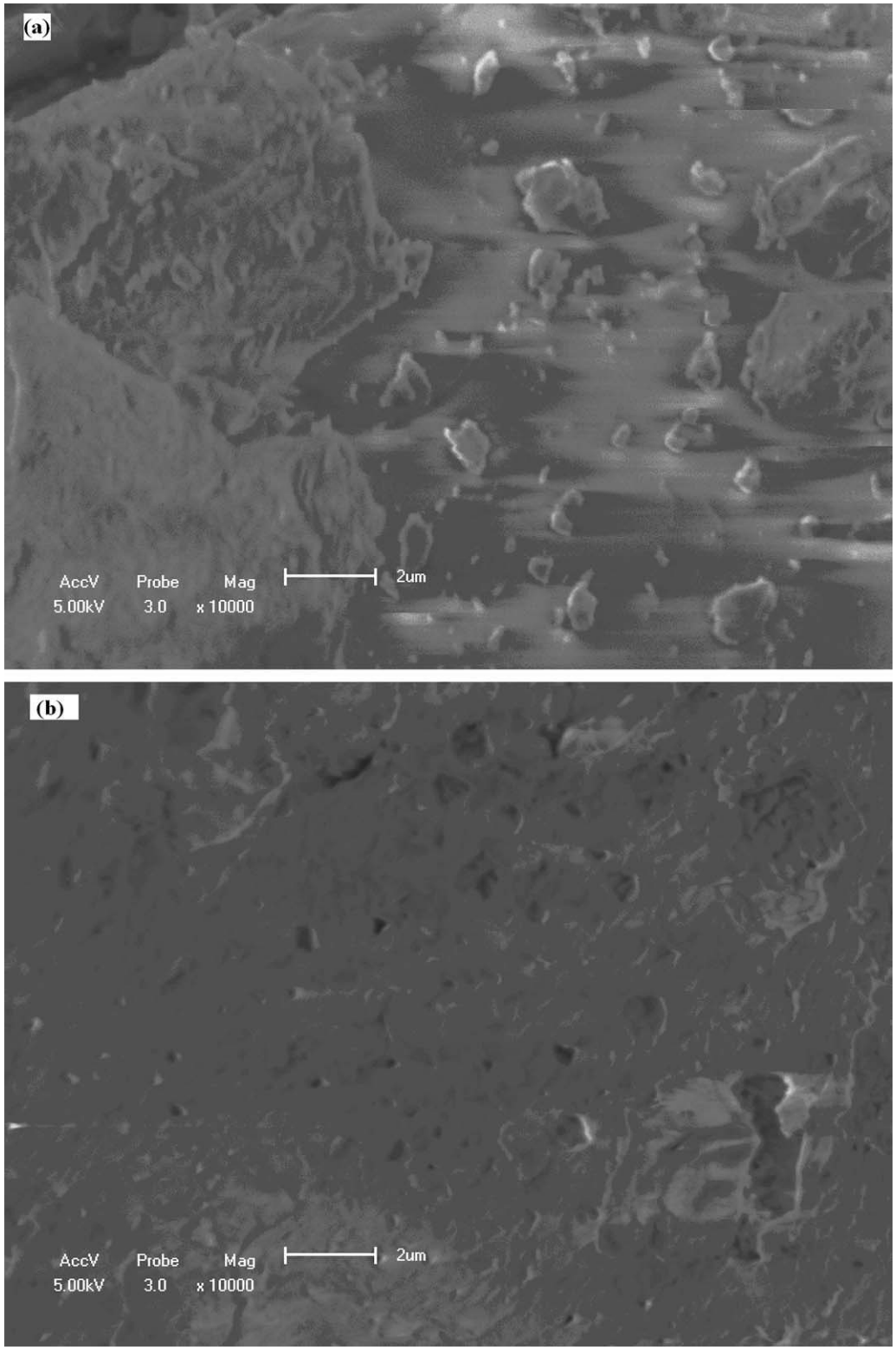

Figure 1 10,000× magnification SEM micrographs of as-synthesized $BaAl_xO_y$:Eu^{2+},Dy^{3+} with Eu^{2+}:Dy^{3+} ratio = (a) 10 : 1 (b) 1 : 10.

as a result of transitions in either 4f energy levels, $4f^{n-1}5d^1$ states or charge-transfer states. In the case of doping with Eu^{2+} ions, luminescence is due to $4f^7 \rightarrow 4f^6 5d^1$ transitions in Eu^{2+}. 4f↔5d transitions are electric dipole allowed optical transitions and correspond to strong optical absorption. During excitation, 4f electrons get transferred to the 5d orbital, which is split into a number of levels due to the

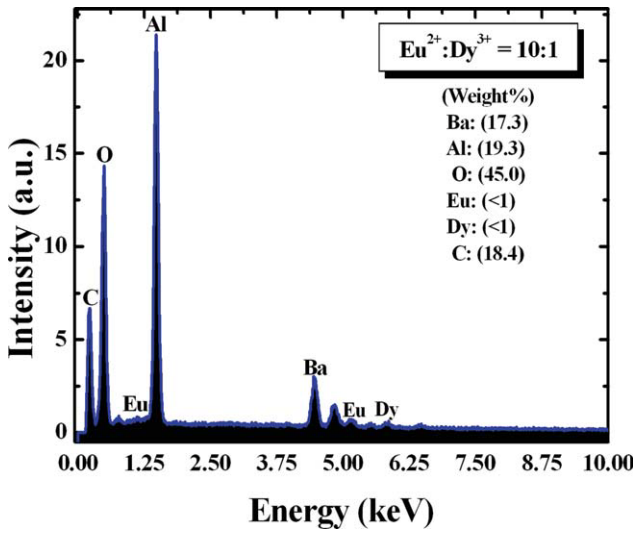

Figure 2 EDS spot analysis results for the $BaAl_xO_y:Eu^{2+},Dy^{3+}$ powder sample with 10 : 1 $Eu^{2+}:Dy^{3+}$ ratio. [Color figure can be viewed in the online issue, which is available at wileyonlinelibrary.com.]

crystal field. The 4f electrons of Eu^{2+} are not sensitive to the lattice environment due to the shielding function of the outer shell, but the 5d electrons may couple strongly to the lattice. Consequently, the mixed states of 4f5d will be split by the crystal field and will couple strongly to the lattice phonons, resulting in broadband absorption and emission. On the other hand, it is known that different host structures and crystallographic distortions will influence the crystal field environment of rare earth ions in the host structure.[24] Since the crystal field splitting varies considerably depending upon the host material, the spectral position of the excitation band would also change. In this work the excitation spectrum at each concentration is broad with a peak at 340 nm. A concentration-dependent shoulder also appears at 275 nm.

The PL curves for the phosphor materials (Fig. 4) show that the maximum peak wavelength of the phosphorescence does not vary significantly with the concentration of the dopants. This implies that the crystal field, which affects the 5d electron states of the Eu^{2+} ions, is not changed dramatically by the concentration variations in the phosphors. Unlike the excitation bands, the emission bands do not only depend on the crystal field splitting of the 5d level and the 4f→5d de-excitations. In a given host, the emission of Eu^{2+} is also significantly influenced by the size of the host cation (Ba^{2+} in this case), which is replaced by Eu^{2+}. The ionic size of Eu^{2+} (1.20 Å) is smaller than the radius of the Ba^{2+} ion (1.38 Å). Hence, when Eu^{2+} substitutes for Ba^{2+} in $BaAl_xO_y$, the Eu^{2+} ion experiences a reduced attraction owing to shrinkage of the crystal lattice. Anamorphic crystal lattices result when the surroundings of Eu^{2+} are changed and so the emission wavelengths change correspondingly.[6,25]

Two Ba^{2+} sites are believed to exist in the $BaAl_2O_4$ crystal structure. However, the symmetry and non-winding emission bands in the observed results illustrate the existence of one kind of luminescent center in the $BaAl_xO_y:Eu^{2+},Dy^{3+}$,where the Eu^{2+} ions are substituted with the nine-coordinated Ba^{2+} sites.[26] Of the two expected Ba^{2+} sites, the first one (2a) has a multiplicity of two and a site symmetry of C_3 while the second one (6c) has a multiplicity of six

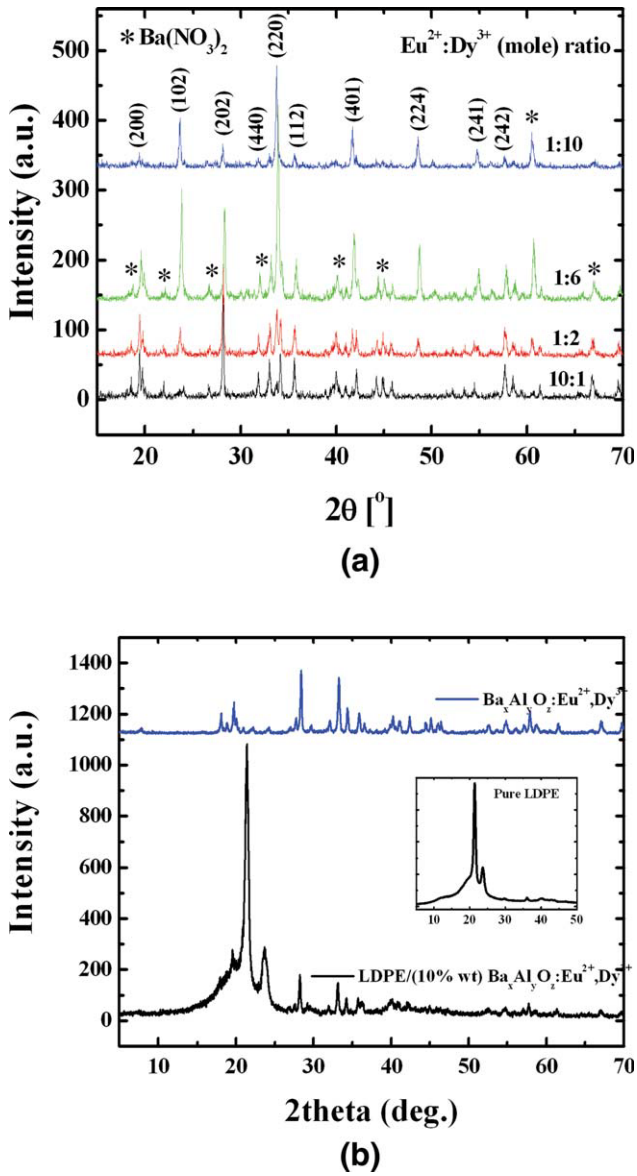

Figure 3 (a) XRD spectra of $BaAl_xO_y:Eu^{2+},Dy^{3+}$ powder samples for various $Eu^{2+}:Dy^{3+}$ ratios (b) XRD spectra of $BaAl_xO_y:Eu^{2+},Dy^{3+}$ phosphor sample with $Eu^{2+}:Dy^{3+}$ molar ratio = 2 : 1, and composite of LDPE with 10% $BaAl_xO_y:Eu^{2+},Dy^{3+}$. Inset - XRD spectrum of pure LDPE. [Color figure can be viewed in the online issue, which is available at wileyonlinelibrary.com.]

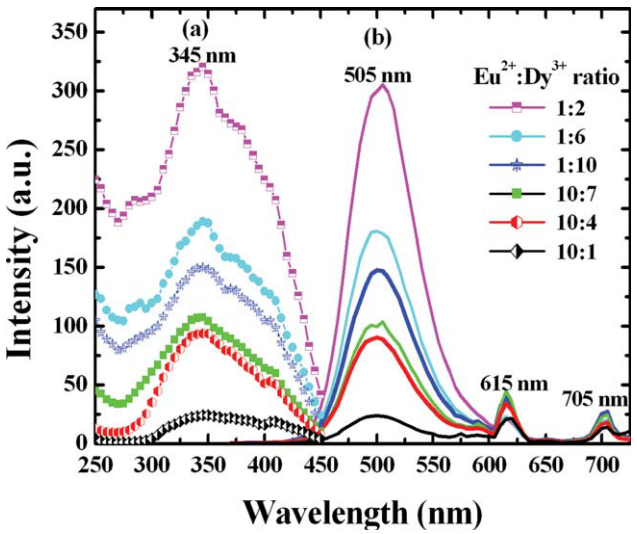

Figure 4 PL (a) excitation λ_{em} = 505 nm and (b) emission λ_{exc} = 340 nm, spectra of $BaAl_xO_y:Eu^{2+},Dy^{3+}$ phosphor for Eu^{2+}:Dy^{3+} ratio = 10 : 1 - 1 : 10. [Color figure can be viewed in the online issue, which is available at wileyonlinelibrary.com.]

and a site symmetry of C_1. Both the Ba^{2+} sites have nine-coordination and the sites are similar in average size (d(Ba-O)Ave = 2.86 and 2.87 Å). However, the lower symmetry site has also shorter Ba-O distances (2.69 Å) corresponding to those typical of Eu^{2+}-O (2.68 Å[27]). These differences imply that the 6c site will be filled preferentially leading to a corresponding higher PL intensity as a result of a contribution from six instead of two Eu^{2+} ions. The emission wavelength (505 nm) is consistent with the result derived from the ceramic method by Lin et al.[24] but slightly higher than the 500 nm obtained by Stefani et al.,[28] who also observed a minor peak at 435 nm, using the solid state reaction method and Ryu et al. (solid state synthesis)[29] as well as the 496 nm by Guanming et al. (microemulsion method).[30]

Though the mechanism of persistent luminescence in lanthanide ions-doped alkaline earth aluminates is not fully understood, it is agreed that the Eu^{2+} ion is the luminescent center while the R^{2+} and R^{3+} ions have been suggested to trap holes and electrons, respectively.[31] The mechanism is considered to include the photoionization of the Eu^{2+} ions and a subsequent transfer of the electrons to traps formed by the lattice defects as oxide ion vacancies and possibly also the auxiliary R^{3+} ion codopants. The thermal bleaching of the electrons from the traps followed by the process reverse to the storage of the excitation energy leads to the Eu^{2+} emission.[32]

The mechanisms explaining the enhanced luminescence emission, as well as the photoluminescence quantum efficiency when nanoparticle-filled polymer composites act as the active emitting layer, are not particularly clear. Initially, optical scattering from the nanoparticle surfaces was believed to be a factor but was excluded since it could not explain some phenomena such as the observed radiance enhancement in LEDs.[33] An alternative possible explanation was in terms of an increase of the recombination at the polymer-nanoparticle interfaces, but this was also discounted. A more plausible mechanism suggests that the change in morphology, arising from a significant increase in surface area, may be responsible for the observed enhanced luminance.[33,34] The high surface reactivity of a nanostructure with a polymer may provide interactions that can modify polymer properties and defect formation in a positive way, leading to novel luminescent properties of the composite. These interactions may yield new radiative recombination mechanisms which may be utilized for broadband light emission or wavelength tunable emission. These mechanisms may be influenced by factors such as the individual properties of the organic and inorganic components as well as their relative concentration. In some nanocomposites, the existence of new recombination mechanisms is suggested by the generation of new PL emission lines,[35] which may be attributed to the formation of interfacial states termed exciplex.[36]

Decay curves

Figure 6 depicts the typical afterglow decay curves of the phosphor samples after the powders were activated using a pulsed xenon lamp. The curves show that the $BaAl_xO_y:Eu^{2+},Dy^{3+}$ phosphor material emits light far longer than the typical microsecond

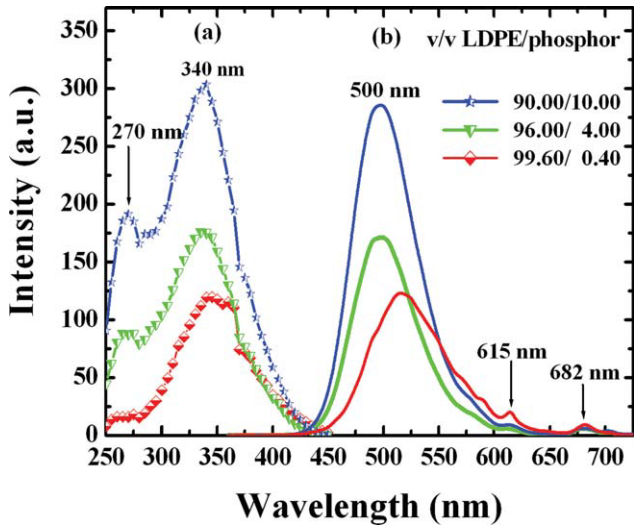

Figure 5 PL (a) excitation λ_{em} = 500 nm and (b) emission λ_{exc} = 340 nm, spectra of LDPE/$BaAl_xO_y:Eu^{2+},Dy^{3+}$ composites for Eu^{2+}:Dy^{3+} ratio = 1 : 2. [Color figure can be viewed in the online issue, which is available at wileyonlinelibrary.com.]

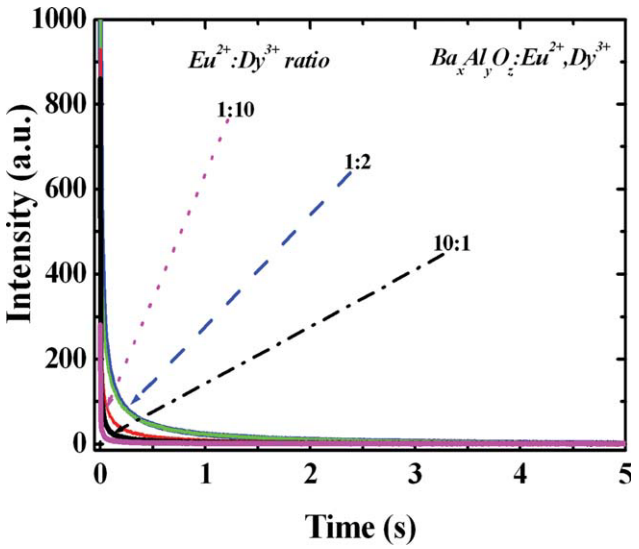

Figure 6 Decay curves of $BaAl_xO_y:Eu^{2+},Dy^{3+}$ phosphor for the samples with $Eu^{2+}:Dy^{3+}$ molar ratios = 10 : 1 - 1 : 10. [Color figure can be viewed in the online issue, which is available at wileyonlinelibrary.com.]

lifetime of Eu^{2+}.[37] This indicates the presence of persistent luminescence. The origin of this long persistence is associated with the second activator ion Dy^{3+}. The Dy^{3+} incorporation creates deep traps in the energy band gap of the $BaAl_xO_y:Eu^{2+},Dy^{3+}$. These traps are in the form of hole-trapping levels near the valence band. After excitation by the light photons, electrons of the Eu^{2+} ion in the 4f level transfer to the 5d level, and holes are produced in the valence band. Some holes created are captured by the Dy^{3+} hole traps, then thermally released slowly to the valence band, and returned to the ground state of Eu^{2+} accompanied with the emission of light photons.

It can be clearly seen that all the afterglow decay curves are composed of two regimes, i.e., the initial rapid decay followed by a much slower process. The initial luminescent intensity and decay speed of afterglow of phosphors are different from each other. Decay times can be calculated by a curve fitting technique based on the following equation:

$$I = A_1 \exp\left(-\frac{t}{\tau_1}\right) + A_2 \exp\left(-\frac{t}{\tau_2}\right), \qquad (2)$$

where I is the phosphorescence intensity, A_1 and A_2 are constants, τ_1 and τ_2 are decay times for the exponential components, and t is time.[38] The results recorded in Tables I and II indicate that the $BaAl_xO_y:Eu^{2+},Dy^{3+}$ phosphor samples had different decay times.

TABLE I
Results for Fitted Decay Curves of the Phosphor Powders

Sample ($Eu^{2+}:Dy^{3+}$)	10 : 1	1 : 2	1 : 10
Component		Half life times (s)	
Fast (τ_1) [$\times 10^{+4}$]	3.3	3.4	0.4
Slow (τ_2) [$\times 10^{+3}$]	7.8	8.8	2.6

TABLE II
Results for Fitted Decay Curve of the 0.4 Vol. % LDPE/BaAlxOy:Eu2+,Dy3+ Composite—Taken from 1 : 2, Eu2+:Dy3+ Ratio

Component	Fast (τ_1) [$\times 10^{+2}$]	Medium (τ_2) [$\times 10^{+2}$]	Slow (τ_2) [$\times 10^{+2}$]
Half life times (s)	0.7	13.53	155.28

The role of Eu^{2+} ions as well as Dy^{3+} ions as luminescent centers and trap centers, respectively, in aluminate phosphors is well established. The lifetime of afterglow is related to the energy stored in the trap level and the number of electrons which stay in the trap level. The intensity of the afterglow is related to the velocity, including the velocity of electrons escaping from the trap level and the velocity of energy transfer. The rapid-decaying process is due to the short survival time of the electrons in Eu^{2+} while the slow-decaying process arises from the deep trap energy center of Dy^{3+}.[39] The magnitude of the afterglow intensity and decay time depend on the type of the host structure, which influences the nature of traps formed.

The curves for the polymer-phosphor nanocomposites, displayed in Figure 7, reveal very interesting observations. At a phosphor content of only 0.4 vol. %, the polymer matrix seems to alter the decay mechanism from second order to third order as the

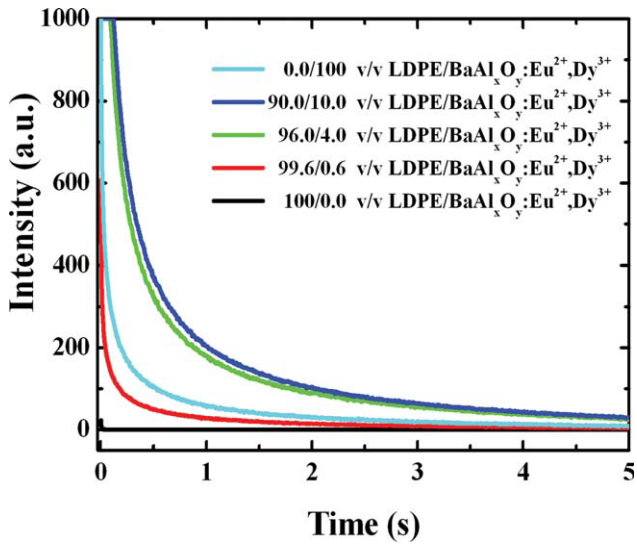

Figure 7 Decay curves of pure LDPE, LDPE/$BaAl_xO_y:Eu^{2+},Dy^{3+}$ nanocomposites for phosphor vol.% = 0.4 - 10 and $BaAl_xO_y:Eu^{2+},Dy^{3+}$ phosphor sample with $Eu^{2+}:Dy^{3+}$ molar ratio = 2 : 1. [Color figure can be viewed in the online issue, which is available at wileyonlinelibrary.com.]

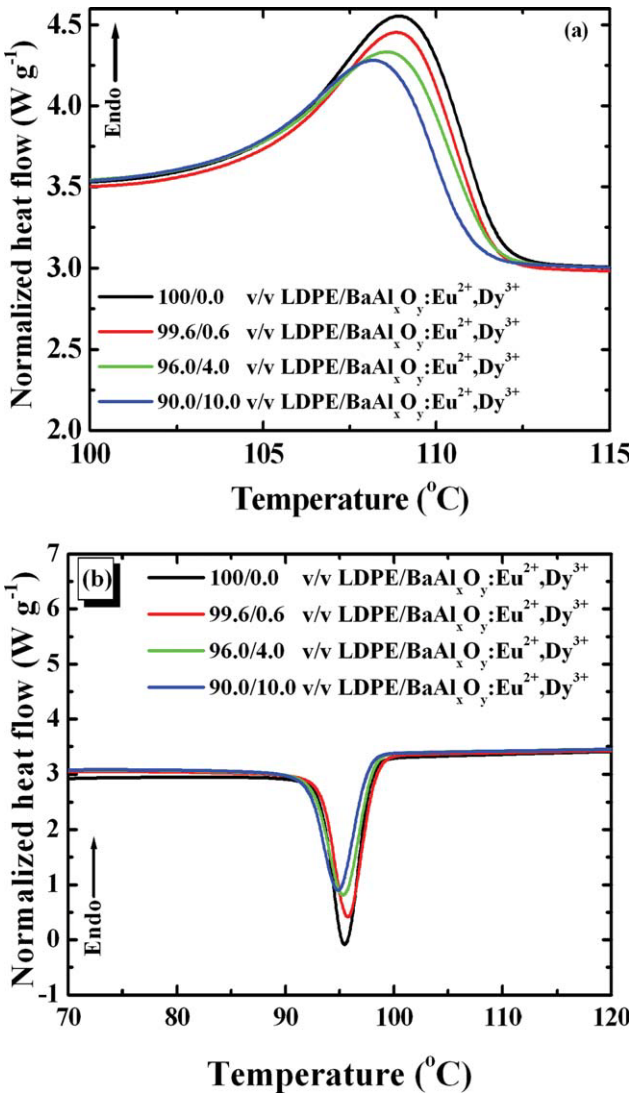

Figure 8 DSC (a) heating and (b) cooling curves of LDPE and LDPE/$BaAl_xO_y$:Eu^{2+},Dy^{3+} nanocomposites. [Color figure can be viewed in the online issue, which is available at wileyonlinelibrary.com.]

corresponding decay curves could be fitted with the third order exponential equation [eq. (3)],

$$I = A_1 \exp\left(-\frac{t}{\tau_1}\right) + A_2 \exp\left(-\frac{t}{\tau_2}\right)) + A_3 \exp\left(-\frac{t}{\tau_3}\right). \quad (3)$$

In addition, further increase of the phosphor content above 0.4% appears to progressively slow the rate of decay. Such elongation in afterglow characteristics would be very appropriate for applications such as lighting, among others. As mentioned earlier on (PL section), the origin of the influence of the polymer on phosphorescence may be rooted in the morphological changes that arise from the increased surface area.[33,34] The contribution of hole mobility in this process may be significant and is worth considerating. It has been proposed that when nanoparticles are introduced into a polymer, probable causes for the improvement in hole mobility may be either a reduction in the density of traps or reduction in charge trapping due to the superposition of several transport mechanisms in the nanocomposite, which may include percolation through polymer nanoparticle interface network.[40] A low rate of hole mobility and electron-hole recombination will increase the retrapping probability and further slow down the decay process.[41]

Thermal properties

The DSC heating and cooling curves of the pure LDPE and the LDPE- $BaAl_xO_y$:Eu^{2+},Dy^{3+} nanophosphor composites obtained from the second heating and cooling cycles, respectively, are shown in Figure 8. The observed as well as expected parameters corresponding to these DSC curves are recorded in Table III. The curves show that as the phosphor content is increased, both the melting and crystallization temperatures decrease slightly. The reduced temperature values are an indication of a reduction in crystallite sizes in LDPE. This result is similar to our previous observations on the effect of the commercial $SrAl_2O_4$:Eu^{2+},Dy^{3+} phosphor in LDPE.[14] However, in contrast to the same work, values of the expected melting enthalpy values (normalized with respect to the mass fraction of the LDPE in the composite), are lower than the experimentally determined ones. Although the difference in the two values progressively decreases as the phosphor content increases, it is clear that the $BaAl_xO_y$:Eu^{2+},Dy^{3+} particles acted as nucleating centers

TABLE III
DSC Data of LDPE and Its LDPE/BaAlxOy:Eu2+,Dy3+ Composites

Filler content (Vol. %)	T_m/°C ± σ	ΔH_m^{obs}/Jg^{-1} ± σ	ΔH_m^{cal}/Jg^{-1}	T_c/°C ± σ	ΔH_c^{obs}/Jg^{-1} ± σ	ΔH_c^{cal}/Jg^{-1}
0.0	109.2 ± 0.0	52.3 ± 7.9	–	95.4 ± 0.1	−64.16 ± 6.5	–
0.4	109.2 ± 0.2	57.1 ± 7.5	52.1	95.6 ± 0.1	−63.9 ± 2.7	−63.9
4.0	109.2 ± 0.7	53.3 ± 1.3	50.3	95.2 ± 0.2	−64.7 ± 2.6	−61.7
10.0	108.3 ± 0.3	48.6 ± 5.5	47.4	95.1 ± 0.2	−57.4 ± 5.5	−58.2

T_m: melting peak temperature; T_c: crystallization peak temperature; ΔH_m and ΔH_c: melting and crystallization enthalpies, respectively; σ: standard deviation.

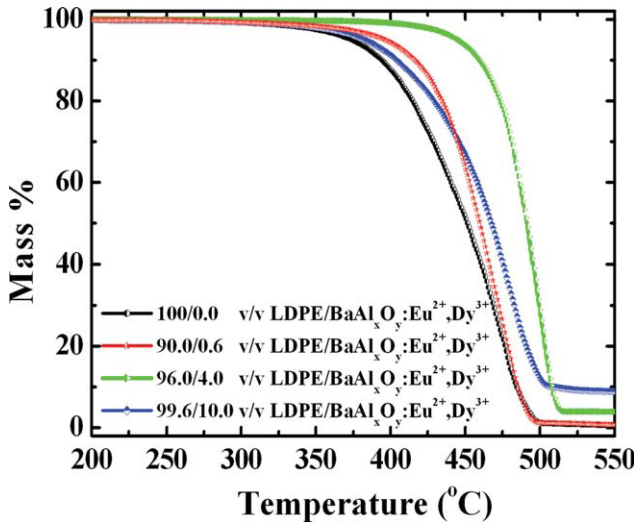

Figure 9 TGA curves for LDPE and LDPE/$BaAl_xO_y:Eu^{2+},Dy^{3+}$ nanocomposites. [Color figure can be viewed in the online issue, which is available at wileyonlinelibrary.com.]

and enhanced the overall crystallinity in the LDPE nanocomposite while preventing lamellar growth. This is in line with some documented results[42] for the effect of nanostructured fillers.

Previous studies have shown that the thermal stability of LDPE can be enhanced to various extends following the introduction of phosphor nanoparticles.[14] In this work, TGA measurements were made to investigate the effect of the combustion-synthesized $BaAl_xO_y:Eu^{2+},Dy^{3+}$ phosphor nanoparticle fillers on the thermal stability of LDPE. The curves obtained from the measurements are depicted in Figure 9. The curves show that $BaAl_xO_y:Eu^{2+},Dy^{3+}$ significantly increased the thermal stability of LDPE, shifting the onset temperature of degradation from about 324°C to 400°C (for the nanocomposite with 4 vol. % of $BaAl_xO_y:Eu^{2+},Dy^{3+}$). Two probable reasons may account for the improved stability. Firstly, a strong interaction between the nanofiller particles and the polymer chains may result in reduced chain mobility, which then suppresses the chain transfer reaction that is responsible for the degradation,[43] ultimately delaying the onset temperature of mass loss. The 10 vol. % sample shows that there is a filler loading threshold for improved stability. However, the afterglow curves indicate that this particular concentration does not perform much better than the 4 vol. % one, indicating that the threshold filler content for optimum persistence luminescence in this system was less than 10%.

CONCLUSIONS

To optimize the luminescence properties of a phosphor, for incorporation in a polymer matrix, nanostructured $BaAl_xO_y:Eu^{2+},Dy^3$ powders were prepared by a combustion method and ultimately mixed in an LDPE matrix. EDS analysis confirmed the elemental composition in the phosphor. The average crystallite sizes determined from XRD measurements, using the Scherrer formula, ranged between 34 and 41 nm. The powders exhibited high brightness luminescence with major peaks having maxima at 505 nm, which were nicely replicated by the nanocomposite samples. Additionally, the persistence luminescence behavior of the phosphor/polymer composites were observed to be profoundly enhanced compared with that of the phosphor alone. The enhancement probably originated in the change in morphology, arising from the significant increase in surface area. DSC results show that the $BaAl_xO_y:Eu^{2+},Dy^{3+}$ particles acted as nucleating centers and enhanced the overall crystallinity in the LDPE nanocomposite while preventing lamellar growth. The LDPE-$BaAl_xO_y:Eu^{2+},Dy^3$ nanocomposites had higher thermal stability with respect to that of the pure LDPE. The improved stability may be attributed to a strong interaction between the nanofiller particles and the polymer chains, which led to reduced chain mobility, ultimately delaying the onset of degradation

The Centre of Microscopy and the Department of Geography (University of the Free State) are acknowledged for SEM and XRD measurements, respectively.

References

1. Blasse, G.; Grabmaier, B. G. Luminescent Materials; Springer-Verlag: Berlin, 1994.
2. Feldmann, C.; Justel, T.; Ronda, C. R.; Schmidt, P. J Adv Funct Mater 2003, 13, 511.
3. Vetrone, F.; Boyer, J. C.; Capobianco, J. In A Handbook of Luminescence, Display Materials, and Devices; Nalwa, H. S., Rohwer, L. S., Eds.; American Scientific Publishers: Stevenson Ranch, CA, 2003; Vol. 2, p 141.
4. Matsuzawa, T.; Aoki, Y.; Takeuchi, N.; Murayama, Y. J Electrochem Soc 1996, 143, 2670.
5. Kuang, J.; Liu, Y. L. Chem Lett 2005, 34, 598.
6. Mothudi, B. M.; Ntwaeaborwa, O. M.; Botha, J. R.; Swart, H. C. Phys B: Condens Matter 2009, 404, 4440.
7. Katsumata, T.; Sakai, R.; Komuro, S.; Morikawa, T.; Kimura, H. J. Cryst Growth 1999, 198, 869.
8. Zou, G. F.; Li, H.; Zhang, Y.; Qian, Y. T. Nanotechnology 2006, 17, S313.
9. Bang, J.; Abboudi, M.; Abrams, B.; Holloway, P. H. J Lumin 2004, 106, 177.
10. Colvin, V. L.; Schlamp, M. C.; Alivisatos, A. P. Nature (London) 1994, 370, 354.
11. Kagan, C. R.; Mitzi, D. B.; Dimitrakopoulos, C. D. Science 1999, 286, 945.
12. Huynh, W. U.; Dittmer, J. J.; Alivisatos, A. P. Science 2002, 295, 2425.
13. Chang, C. C.; Chen, W. C. Chem Mater 2002, 14, 4242.
14. Bem, D. B.; Luyt, A. S.; Dejene, B. F.; Botha, J. R.; Swart, H. C. Phys B: Condens Matter 2009, 404, 4504.

15. Klug, H. P.; Alexander, L. E. In X-ray Powder Diffraction Procedures; Wiley: New York, 1959.
16. Cohen, D.; Sorrell, C. C.; Dou, S. X.; Apperley, M. J. J Am Ceram Soc 1991, 74, 1541.
17. Kang, Y. C.; Lenngoro, I. W.; Park, S. B.; Okuyama, K. Mater Res Bull 2000, 35, 789.
18. Chang, H.; Lenggoro, I. W.; Okuyama, K.; Kim, T. O. Jpn J Appl Phys 2004, 43, 3535.
19. Jacobsohn, L. G.; Bennett, B. L.; Muenchausen, R. E.; Smith, J. F.; Cooke, D. W. Radiat Meas 2007, 42, 675.
20. Lee, S. K.; Yoon, H. H.; Park, S. J.; Kim, K. H.; Choi, H. W. J. J Appl Phys 2007, 46, 7983.
21. Ryu, H.; Singh, B. K.; Bartwal, K. S. Phys B: Condens Mater 2008, 403, 126.
22. Chen, X. Y.; Ma, C.; Li, X. X.; Shi, C. W.; Li, X. L.; Lu, X. D. R. J Phys Chem 2009, 113, 2685.
23. Lu, C. H.; Chen, S. Y.; Hsu, C. H. Mater Sci Eng B 2007, 140, 218.
24. Lin, Y.; Zhang, Z.; Tang, Z. Mater Chem Phys 2001, 70, 156.
25. Chen, Y. J.; Qiu, G. M.; Sun, Y. B. J Rare Earths 2002, 20, 50.
26. Park, Y. J.; Kim, Y. J Mater Sci Eng B 146: 84 2008.
27. Shannon, R. D. Acta Crystallogr 1976, A32, 751.
28. Stefani, R.; Rodrigues, L. C. V.; Carvalho, C. A. A.; Felinto, M. C. F. C.; Brito, H. F.; Lastusaari, M.; Hölsä, J. Opt Mater 2009, 31, 1815.
29. Ryu, H.; Singh, B. K.; Bartwal, K. S. J Lumin 1999, 85, 149.
30. Guanming, Q.; Yongjie, C.; Xiujuan, G.; Linjiu, X.; Yiguang, T.; Yanbin, S. J Rare Earths 2005, 23, 5.
31. Aitasalo, T.; Deren, P.; Holsa, J.; Jungner, H; Krupa, J. C.; Lastusaari, M.; Legendziewicz, J.; Niittykoski, J.; Strek W. J Solid State Chem 2003, 171, 114.
32. Aitasalo, T.; Hölsä, J.; Jungner, H.; Lastusaari, M.; Niittykoski, J. J Phys Chem B 2006, 110, 4589.
33. Blom, P. W. M.; Schoo, H. F. M.; Matters, M. Appl Phys Lett 1998, 73, 3914.
34. Carter, S. A. Appl Phys Lett 1998, 71, 9.
35. Aleshin, A.; Alexandrova, E.; Shcherbakov, I. J Phys D: Appl Phys 2009, 42, 1361.
36. Morteani, A.; Ho, P.; Friend, R.; Silva, C. Appl Phys Lett 2005, 86, 1077.
37. Poort, S. H. M.; Meijerink, A.; Blasse, G. J Phys Chem Solids 1997, 58, 1451.
38. Matsuzawa, T.; Nabae, T.; Katsumata, T.; Sasajima, T. J Electrochem Soc 1997, 144, L243.
39. Katsumata, T.; Nabae, T.; Sasajima K. J Cryst Growth 1998, 183, 361.
40. Aleshin, A.; Shcherbakov, I.; Alexandrova, E.; Lebedev, E. Solid State Commun 2008, 146, 161.
41. Jia, W.; Yuan, H.; Lu, L.; Liu, H.; Yen, W. M. J Lumin 1998, 76, 424.
42. Ning, N. Y.; Yin, Q. J.; Luo, F.; Zhang, Q.; Du, R.; Fu, Q. Polymer 2007, 4, 7374.
43. Luyt, A. S.; Dramicanin, M. D.; Antic, Z.; Djokovic, V. Polym Test 2009, 28, 8.